Journal of Petroleum Science and Engineering 179 (2019) 1063–1077

Contents lists available at ScienceDirect

Journal of Petroleum Science and Engineering

journal homepage: www.elsevier.com/locate/petrol

Evaluating chemical-scale-inhibitor performance in external magnetic fields using a dynamic scale loop

Ammar Al Helal[a,b,*], Adam Soames[a], Stefan Iglauer[c], Rolf Gubner[a], Ahmed Barifcani[a]

[a] WA School of Mines: Minerals, Energy and Chemical Engineering, Curtin University, Perth, W.A, Australia
[b] Al-Khawarizmi College of Engineering, University of Baghdad, Jadriyah, Baghdad, Iraq
[c] Petroleum Engineering Department, Edith Cowan University, Joondalup, W.A, Australia

Keywords:
Monoethylene glycol
Chemical scale inhibitor
Magnetic-field treatment
Scale formation
Electrical conductivity
Zeta potential

A B S T R A C T

Monoethylene glycol (MEG) is extensively used in oil and gas pipelines to prevent the formation of gas hydrates. However, the injection of MEG may inadvertently contribute to mineral-ion precipitation through reduced solubility of ionic species and operation under alkaline conditions for corrosion control. As a result, the injection of chemical scale inhibitors (CSI) to manage scaling is often required. Non-chemical inhibitors, such as external magnetic fields (MFs) have also been shown to inhibit scaling in aqueous solutions. With this in mind, we investigated the combined application of CSIs and MF treatment to study the formation of scale under conditions representative of a MEG regeneration system's reboiler, a system under a high risk of scale formation. Two commercial CSIs were examined in the presence and absence of a 0.650-T external MF using a dynamic-scale-loop device. The CSIs were injected into ionic solutions containing 1656.9 ppm calcium ions and 2628 ppm carbonate ions in aqueous MEG (80 vol%), and experiments were performed at 130 °C and pH 9.5. Despite the presence of a CSI, the MF promoted scale formation and afforded a stable calcium carbonate phase morphology at high MEG concentrations. Moreover, the zeta potential under the applied MF was lower than that in the absence of the MF, which led to greater scaling, implying that the magnetic field had an ionic interfacial effect. These results provide significant insight into the effect of a MF on scale formation, irrespective of the use of a CSI, and help to interpret the effects of various treatments for scale removal or the prevention of scale formation during the MEG regeneration process.

1. Introduction

Inorganic deposits (scale) in oil and gas pipelines are one of the most critical problems encountered in the oil and gas industry owing to their direct adverse impact on flow assurance, which ultimately leads to a decrease in production (Babu et al., 2015; Wang et al., 2013). Scale can form due to changes in operating conditions; i.e., temperature, pressure, pH, and the use of additives such gas-hydrate inhibitors (Yong and Obanijesu, 2015, BARAKA-Lokmane et al., 2012; Østvold and Randhol, 2001, Flaten et al., 2015). The primary source of mineral ions that form scale is the seawater injected into oil wells or formation water breakthrough during oil production (Shen et al., 2008; Halvorsen et al., 2007). For instance, sulfate scale is formed during recovery operations following the downhole injection of seawater, which is used to increase wellhead pressure and prompt production flow (Amiri et al., 2013; Bader, 2006). Meanwhile, carbonate scales are formed following the breakthrough of formation water through the mixing of different mineral ions, such as calcium, magnesium, and barium, present in the formation water with the carbonate ions formed under alkaline conditions from dissolved CO_2 gas (Halvorsen et al., 2007). On-shore analyses using scanning electron microscopy (SEM), X-ray diffraction (XRD), and chemical analysis have shown that the most common scale deposit in most oil fields is $CaCO_3$ (Flaten et al., 2009; Kan et al., 2005; Yong and Obanijesu, 2015).

Furthermore, during oil and gas recovery operations, gas-hydrate inhibitors are often injected to prevent the formation of hydrates that hinder hydrocarbon flow in transportation pipelines (Yong and Obanijesu, 2015; Brustad et al., 2005; Sandengen, 2006; Tomson et al., 2002; Soames et al., 2018; Halvorsen et al., 2007). However, gas-hydrate inhibitors such as monoethylene glycol (MEG), lower the

Abbreviations: CSI, chemical scale inhibitor; DSL, dynamic-scale-loop device; EC, electrical conductivity; HEDP, 1-hydroxyethane-1,1-diphosphonic acid; MEG, monoethylene glycol; MF, magnetic field; SEM, scanning electron microscopy; XRD, X-ray diffraction

* Corresponding author. WA School of Mines: Minerals, Energy and Chemical Engineering, Curtin University, Perth, W.A, Australia.
E-mail address: 17610661@student.curtin.edu.au (A. Al Helal).

https://doi.org/10.1016/j.petrol.2019.04.093
Received 10 November 2018; Received in revised form 26 April 2019; Accepted 26 April 2019
Available online 05 May 2019
0920-4105/ © 2019 Elsevier B.V. All rights reserved.

solubility of mineral ions, thereby increasing the risk of scale formation inside pipelines operating using MEG injection (Kaasa et al., 2005; Kan et al., 2002; Lu et al., 2010; Halvorsen et al., 2007). Preventing scale formation by changing oil-recovery procedures to avoid the injection of seawater or formation-water breakthrough is complicated. In addition, the mechanical removal of insoluble scale deposits is expensive and requires process shutdown, which can possibly damage pipelines and equipment (Amjad, 2013; Amjad and Albright, 2015). Different strategies have been adopted to decrease the operating cost of mechanical methods for scale removal and non-production time (Graham et al., 2002; Yuan et al., 1998). For instance, chemical scale inhibitors (CSIs) are often injected into the lean MEG solution after the regeneration process to prevent scale formation inside downstream transportation pipelines and injection systems (Flaten et al., 2015; Hyllestad, 2013).

The most commonly used CSIs in the oil and gas industry are organic phosphonates, polyacrylates, phosphates and polyphosphates, phosphate esters, carboxylates, sulfonates, and various other polymers and copolymers of phosphonates (Kan et al., 2005; Tomson et al., 2002; Amjad, 2010; Cavano, 2005). These chemical substances are chosen according to the environments of the oil reservoirs and transportation pipelines (Cavano, 2005; Tomson et al., 2002). The concentration dosage and injection point of the CSI is assessed according to its laboratory performance in brine solution (Amjad, 2010; Kan et al., 2005; Zeng et al., 2013). However, as CSIs affect solution chemistry and pose risks to both the health of the users and the environment, they are often classified according to their health and environmental risks, as well as inhibitory performance (Amjad, 2010). The threshold amount of a CSI for a defined level of inhibition is referred to as “the minimum effective dose” or “minimum inhibitory concentration”, which is typically 0.5–20 ppm (Zeng et al., 2013; Sorbie and Laing, 2004). Nevertheless, the minimum inhibitory concentration for high-temperature and high-pressure fields that suffer from severe scaling can be in the order of a few hundred ppm (Fan et al., 2012; Zeng et al., 2013). 1-Hydroxyethane-1,1-diphosphonic acid (HEDP) and phosphate esters are extensively used in the processing of circulating cooling water and the chemical cleaning of hot surfaces (Zeng et al., 2013; Perez et al., 2016; Racke, 1992). However, there are only a few investigations on the applications of HEDP and phosphate esters to reboilers during MEG regeneration treatment.

Basically, the remaining concentration of CSI in the rich glycol solution reduces the performance of the pretreatment process during the removal of divalent ions at MEG regeneration plant. This poor removal performance leads to the transfer of un-precipitated mineral ions to the reboiler section. To prevent CSI side effects, magnetic treatment in aqueous brine solutions has been suggested by several researchers because it is a low-cost, stand-alone, and eco-friendly alternative scale-treatment method (Luo and Nguyen, 2017; Esmaeilnezhad et al., 2017; Chibowski and Szcześ, 2018). Previous reports have described the strong potential of magnetic fields (MFs) for a variety of applications; however, the results are often difficult to reproduce (Luo and Nguyen, 2017; Esmaeilnezhad et al., 2017; Chibowski and Szcześ, 2018). Nevertheless, some results are impressive (Rajczykowski and Loska, 2018); for example, Higashitani, Iseri, Okuhara, Kage and Hatade (Higashitani et al., 1995) noted that the zeta potentials (ζ) of colloids were reduced after exposure to a MF, which accelerates coagulation rates; consequently, sediments are more likely to form.

On the other hand, Chang and Weng (2006) reported that the size of a water cluster can be controlled by the application of an external MF. Other studies have indicated that $CaCO_3$ particles form scale with different morphologies and tend to form aragonite in magnetized water than in ordinary water (Chang and Tai, 2010; Tai et al., 2008, 2011). Moreover, it has been shown that MF treatment can significantly inhibit or promote $CaCO_3$-scale formation in an aqueous solution, depending on the anionic and cationic concentrations in the brine solution (AL Helal et al., 2018). Therefore, a MF can control $CaCO_3$ precipitation, thereby serving as a scale-formation inhibitor that decreases the precipitation of divalent ions in an aqueous solution. Consequently, both CSIs and MFs create favorable conditions for low scale growth, resulting in less-severe scaling issues in aqueous solutions. However, the performance of external MF treatment has not been investigated in non-aqueous solutions in the presence of CSIs because of its lack of applicability to the oil and gas industry.

Chemical reactions that involve radical intermediates can be affected by external magnetic fields (Chibowski and Szcześ, 2018), which appear to alter their rates of reaction, product yields, and chemical equilibria (Rodgers, 2009; Steiner and Ulrich, 1989). These reactions have been investigated extensively in aqueous and organic-liquid phases (Scott, 2012; Messiha et al., 2015; Kochmarsky, 1996) and have been described by the radical-pair mechanism (Till and Hore, 1997; Timmel et al., 1998; Chibowski and Szcześ, 2018). This phenomenon is the cornerstone of the spin-chemistry field. Electron-polarization and chemically induced dynamic nuclear (CIDNP) studies have demonstrated the dependency of radical-pair reaction kinetics on the direction of the magnetic field (Till and Hore, 1997). Furthermore, Zeeman interactions between the unpaired electron spins on the radicals and the external magnetic field clearly play essential roles in calcium carbonate formation (Messiha et al., 2015; Parsons et al., 1997; Dhanaraj et al., 2010).

Most previous studies assessed the performance of CSIs under different pressure and temperature conditions using the dynamic-scale-loop-device (DSL-device) method (M. Ramzia et al., 2016; Cole, 2015; Yuan et al., 1998), which involves a tube-blocking system that is used to examine scale formation in capillary tubing coils such as oil and water pipelines (Amjad, 2010; Daniels et al., 2014, AL Helal et al., 2018). The system is recommended for reviewing inorganic scale formation under dynamic conditions (Amjad, 2013; Guan, 2015; Daniels et al., 2014). However, there are few reports on the effects of combined physico-chemical treatments on scale formation, which has been established as the method of choice for examining the behavior of CSIs when exposed to an external MF.

This study aimed to evaluate the effect of an external MF on CSI performance in preventing $CaCO_3$ formation within the reboiler section using 80 vol% MEG solutions during MEG regeneration. The $CaCO_3$ scale-inhibiting performance of CSIs at different concentrations was investigated, and the effect of the MF on the scale-inhibiting performance in a simulated reboiler of a glycolic solution was studied. The DSL technique was used to evaluate the scale-inhibiting performance at 130 °C and 1.0 bar. Furthermore, to evaluate scaling trends following MF treatment, particle-size distributions, ζ potentials, electrical conductivities (ECs), and scale morphologies were determined.

2. Materials and methods

2.1. Brine solutions

The MEG-brine solutions used in this study resemble the compositions of those used in real oil-field situations, as recommended by NACE laboratory screening tests and PSL Systemtechnik (NACE International, 2016, NSTM0374, 2007). The aqueous glycolic solutions consisted of calcium chloride dihydrate (Scharlau reagent grade ACS, > 99 wt%), sodium chloride (Chem-Supply reagent grade, > 99 wt%), sodium carbonate (Chem-Supply reagent grade, 99.7 wt%), MEG solution (Chem-Supply reagent grade, > 99 wt%), etidronic acid (Sigma-Aldrich, 60 wt %), and organophosphates (commercial brand, 30 wt%). An aqueous glycolic solution was used in this study to simulate oil- and gas-pipeline brine solutions. The mineral-ion compositions and their concentrations within the MEG-brine solution are listed in Table 1. The performance of the two types of CSI was evaluated in the laboratory in an external MF using the DSL system at 130 °C and 1.0 bar. The CSI concentrations are listed in Table 2.

Table 1
Feed concentration of cations and anions during DSL testing.

Ion	Anion Solution, *mg/L*	Cation Solution, *mg/L*	Mixed Solution, *mg/L*
Ca^{2+}	0.0	3313.8	1656.9
CO_3^{2-}	5256	0.0	2628
Na+	15005.05	12990.8	13997.9
Cl^-	20033.37	25893.39	22963.4
MEG (vol%)	80	80	80
[a]Ionic Strength, M at 25 °C			0.761
[a]Total Alkalinity, mg/L			10137
pH of the mixed brine solution			9.5

[a] These values were calculated by the Aqion software.

Table 2
CSI concentrations used during DSL testing.

CSI		Dosage Concentration, ppm		
Code	Chemical Name	Low	High	Extremely High
CSI-A	HEDP	20	100	200
CSI–B	Phosphate ester	20	100	200

2.2. Dynamic tube-blocking experiments

Fig. 1 shows a schematic diagram of the DSL system (PSL Systemtechnik, Germany) with the magnetic treatment device. The specifications of the DSL system are listed in Table 3. Commercially available permanent magnets (NdFeB grade SHN45) from Oasis Materials Technology Limited were used in these experiments, and the magnetic flux density was measured using a teslameter (Wutronic, Germany). A permanent magnet was placed around the stainless steel tubing through which the solutions flowed prior to the capillary test coil inside the DSL device. The external magnetic device was designed as a cylinder with an outer diameter of 7.62 cm and a length of 22.86 cm in order to generate a field of approximately 0.65 T with a maximum produced energy (BH_{Max}) of 44.384 MGOe. The cylindrical magnet had a 0.3175 cm hole in the center to allow the brine solution to flow through the MF. Magnetic induction was perpendicular to the flow of the brine solution in this configuration.

The DSL method was used to simulate real conditions within a distillation column when re-concentrating a mixture of brine, CSI, and MEG-rich solutions in the reboiler section. The MEG-rich solution was replaced with a MEG-lean solution during DSL experiments in order to approach the composition of the reboiler solution. CSI performance was evaluated before and after exposure to the external MF at different dosages. The experiments were conducted at 130 °C and 1.0 bar, with 1656.9 ppm of calcium ions as the cationic solution and 2628 ppm of carbonate ions as the anionic solution. The two solutions were prepared separately in two bottles following the standard NACE procedure (NACE International, 2005), filtered, and adjusted to pH 9.5 to enhance scale formation following mixing of the cations and anions.

The stainless steel capillary tubing coil was preheated and set at 130 °C before the commencement of any experiment. The cation and anion solutions were then injected into the DSL system at a constant flow rate of 5 mL/min. The formation of inorganic scale was monitored by PC-interface software that recorded the pressure built up across the capillary tube with time. The maximum pressure across the capillary tube was set to 5.5 bar; the DSL detector terminated the experiment once the pressure sensor detected this value. A two-way valve connected the injection pump lines and the mixing capillary tube coils in order to perform the experiments in magnetic and non-magnetic modes. The data were compared in terms of CSI scale-formation-inhibition performance in a 1-m-long stainless steel coil with an internal diameter

Table 3
DSL specifications.

Component		Specifications	Notes
High-pressure liquid pump	0.1–5.0 mL/min, ± 0.01	Data-logger	
Back pressure valve	0–172 bar, ± 0.01	Stainless steel 316	
Capillary testing coil	1.0 m length 1.41 mm outer diameter 1.01 mm inner diameter	Stainless steel 316	
Mixing coil	1.0 m length 3.17 mm outer diameter 2.01 mm inner diameter	Stainless steel 316	
Pressure detector	1 bar–172 bar	Data-logger	
Heating chamber room	+30 to +250 °C, ± 0.1 °C	Data-logger	
pH meter and the probe	1–14	Data-logger	
Electrical conductivity	0–1000 mS/cm, ± 0.1%	Data-logger	
PC interface	*winDSL* software, Windows 10		

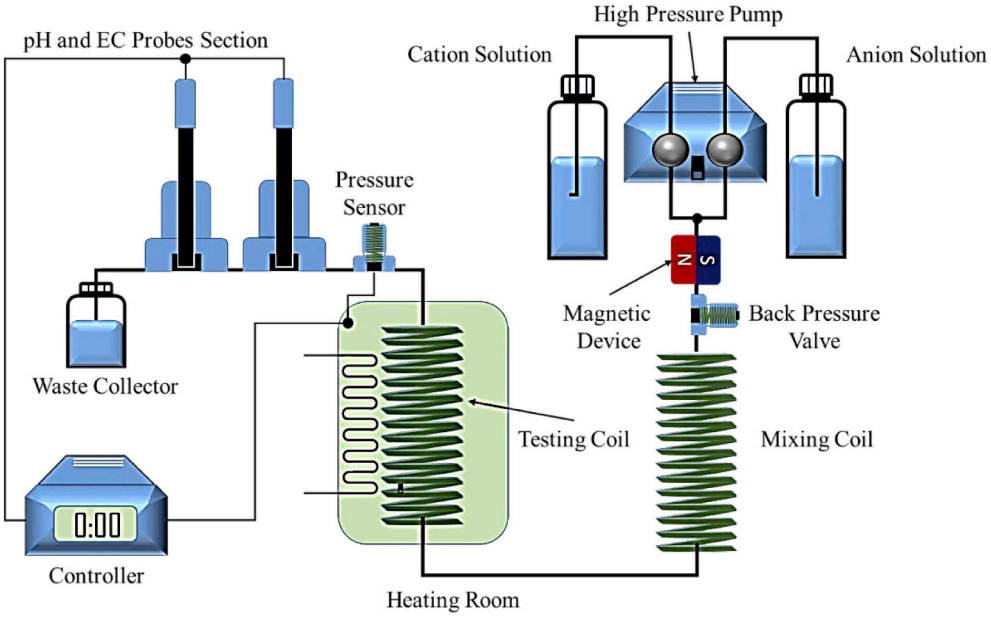

Fig. 1. Schematic diagram of the DSL system.

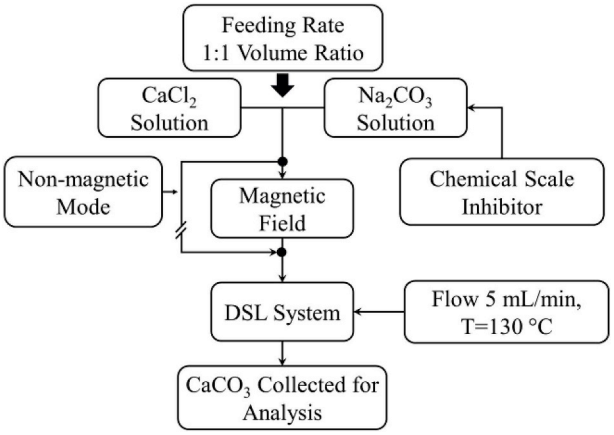

Fig. 2. Experimental flowchart.

(ID) of 1.01 mm.

CSIs were mixed with the anionic solution at twice the specified concentrations because subsequent addition of the cation solution (in a 1:1 vol ratio, as recommended by NACE laboratory screening tests and PSL Systemtechnik) leads to dilution, resulting in adjustment of the CSI concentration to the specified value (see Fig. 2). The CSI concentration for each set was increased gradually, as shown in Table 2. Each experiment was repeated four times to validate the results. All experiments performed without exposure to the MF were repeated using the MF device. The non-CSI experiments were exposed to the MF and the results compared to those from blank experiments. The change in duration time of each experiment is representative of the performance of that CSI in preventing scale formation within the DSL device before and after exposure to the MF. In addition, the $CaCO_3$ solution in the outlet stream was collected for further analysis.

2.3. Analytical method

In this study, the discharge liquid from the DSL was collected for particle-size-distribution and other analyses. The liquid phase was separated from the solid phase by centrifugation of the entire resulting solution. Liquid-phase solutions were subsequently used to measure EC and turbidity, while the solid phases were used to determine ζ potential values; they were also subjected to scanning electron microscopy (SEM; NEON 40EsB FIBSEM, ZEISS NEON) (Fig. 3). The turbidities of the aqueous solutions were measured using a portable turbidity meter (model HI98703-01, HANNA Instruments). Particle-size distributions and ζ potentials were measured following the formation of the $CaCO_3$ scale using a Malvern Panalytical Zetasizer (model ZSP). The $CaCO_3$ morphology was investigated by SEM; samples were coated with a 10-nm-thick platinum layer prior to SEM in order to obtain high-resolution images.

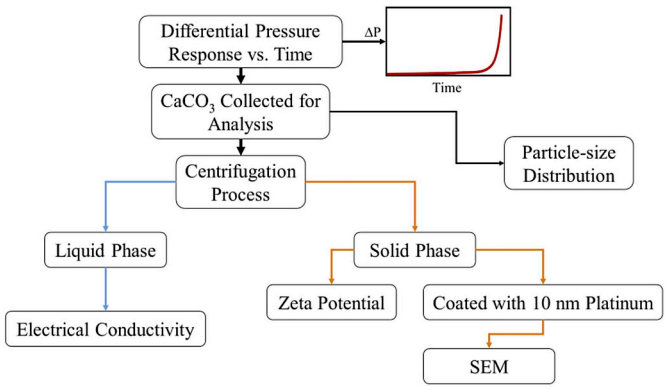

Fig. 3. Flowchart of the scale-formation-analysis protocol for exposed and non-exposed experiments.

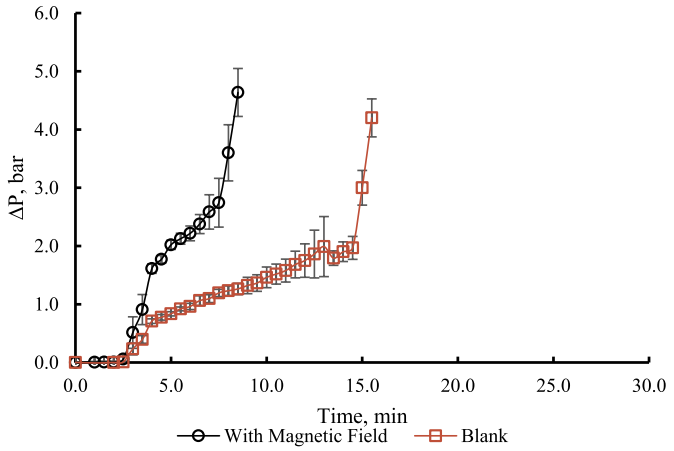

Fig. 4. Changes in pressure (scale formation) as functions of time for calcium and carbonate solutions following exposure, or not, to an applied magnetic field.

3. Results and discussion

3.1. Effect of magnetic field on CSI-free MEG-brine solution

The change in pressure, which is a proxy for scale formation, as a function of time is displayed in Fig. 4, which shows the effect of the MF on scale-formation time after the MEG-brine solution was passed through the cylindrical magnetic device at a field strength of 0.65 T; the results for a corresponding blank MEG-brine test (no MF) are provided for comparison. It is evident from Fig. 4 that the scale-formation rate of the magnetized solution is higher than that of the blank; the difference is significant, with the magnetized solution showing an increase of approximately 45% in scale formation rate. These results are consistent with those of Higashitani and Oshitani (1998), who reported that a MF can promote scale formation in methanolic (water-alcohol) solutions. Furthermore, our results are also consistent with those of Higashitani et al. (1993) who reported that the molecular nucleation frequency can be suppressed by exposure to a MF, while crystals nucleated faster.

Another interesting observation from our study is that the applied MF promoted the formation of scale within 80 vol% MEG solution which implies that the magnetic force was active even after the sample was exposed to a temperature of 130 °C. These outcomes refute the prevailing idea that the MF-memory effect is destroyed by high temperatures (Silva et al., 2015). Moreover, the maximum energy produced by the MF was shown to be more important than the MF strength itself (Chibowski and Szcześ, 2018).

3.2. Effect of magnetic field on CSI-A

Experiments were conducted with different CSI-A concentrations where the solution was exposed to a constant external magnetic strength for 5.0 s to determine the effect of the field on CSI performance. It should be noted that in order to obtain rapid responses, the initial concentrations of anions and cations were relatively high in these experiments. Furthermore, CSIs have been ranked against scale formation in extensive studies in previous years; consequently, such a study was not repeated here, rather, the assessment of overall performance under MF conditions was our focus. The effect of MF strength on the ability of CSI-A, at concentrations of 20, 100, and 200 ppm, to inhibit scale formation is shown in Fig. 5. In the absence of the MF, CSI-A exhibited poor performance at 20 ppm; it failed to impede scale formation (Fig. 5-A). However, the performance of CSI-A consistently

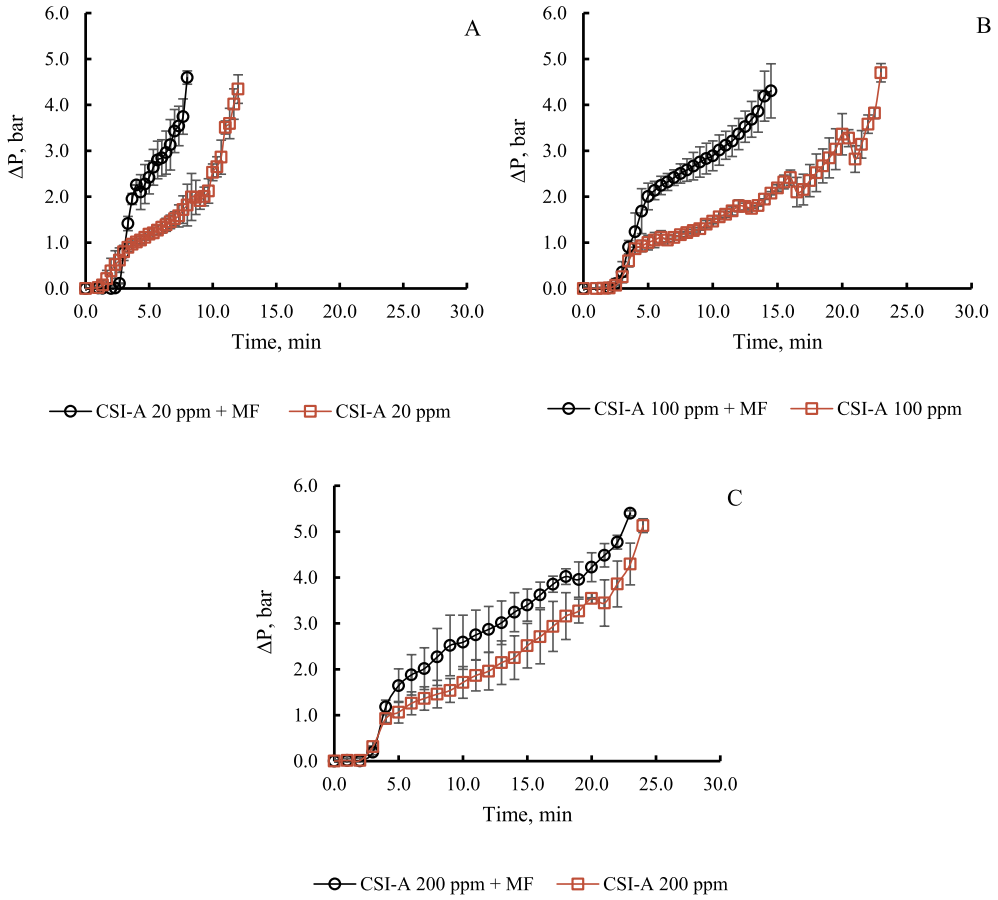

Fig. 5. Changes in pressure (scale formation) as functions of time for calcium and carbonate solutions in the presence of CSI-A at various concentrations following exposure, or not, to an applied magnetic field.

improved at 100 and 200 ppm, with the scale-formation rate reduced by 50% (Fig. 5-B and C). Furthermore, a noticeable difference in the CSI-A performance was observed at all dosages when exposed to the MF; these experiments revealed the inhibiting effect of MF on CSI-A performance, which varied from 33.3% at 20 ppm, to 37% at 100 ppm, and 4% at 200 ppm.

At 200 ppm, CSI-A exhibited an excellent response under the external MF; however, this dosage is very high for industrial use and beyond the limits indicated for this kind of inhibitor (Cavano, 2005). When the effects of different CSI-A concentrations were compared at a constant flow rate of 5.0 mL/min, a significant reduction in CSI-A performance was observed under the applied external MF, which indicates that CSI-A is restricted in preventing scale formation in pipelines when exposed to a MF.

3.3. Effect of magnetic field on CSI–B

The effect of MF strength on the ability of CSI–B, at concentrations of 20, 100, and 200 ppm, to inhibit scale formation is shown in Fig. 6. Irrespective of the inadequate performance of the CSI in inhibiting scale formation, which is evident from Fig. 6-A–C, the results under the external MF are consistent with those obtained for CSI-A; the MF accelerated scale formation at all CSI–B concentrations.

On the other hand, compared to the CSI-A results, those from the MF-exposed and non-exposed trials showed that CSI–B failed to inhibit scale formation. Furthermore, the results discussed in Section 3.1 (in the absence of CSI treatment) and those presented in this section confirmed that CSI–B was inadequate for use as a CSI at such high MEG concentrations and high temperatures. Moreover, a comparison of the blocking times of the blank experiment described in Section 3.1 and the CSI–B experiments presented in this section, which are similar, reveal no changes in scale-formation time before and after the use of CSI–B. In addition, these results show that MF treatment with 80 vol% solutions of MEG significantly advanced scale formation.

3.4. Effect of magnetic field on electrical conductivity

The ECs of CSI-A and CSI–B solutions that were collected before and after exposure to the MF were measured following centrifugation, the results of which are displayed in Fig. 7 for various conditions. These plots reveal that the ECs of the solutions obtained from the magnetized experiments were lower than those obtained from the non-magnetized experiments. Furthermore, a significant reduction in EC was observed for samples from CSI–B concentrations of 100 and 200 ppm, as well 200 ppm of CSI-A. These observations are attributable to differences in the thermodynamic properties of the solutions, leading to changes in the thicknesses of the hydration shells that surround the mineral ions after exposure to the MF. Therefore, the ionic hydration layer was altered, which weakened the electrophoretic effect of the ionic solution. These results are consistent with previous reports; i.e., that the EC of an electrolyte solution is inversely proportional to the thickness of the hydration shell (Higashitani and Oshitani, 1998; Holysz et al., 2007; Szczes et al., 2011).

3.5. Morphology of the formed $CaCO_3$ scale

The mineral deposits produced after each non-exposed experiment were examined by SEM in order to assess changes in morphology. The obtained SEM images were then compared with those of brine solutions prepared at the same concentrations, but subjected to MF. In addition,

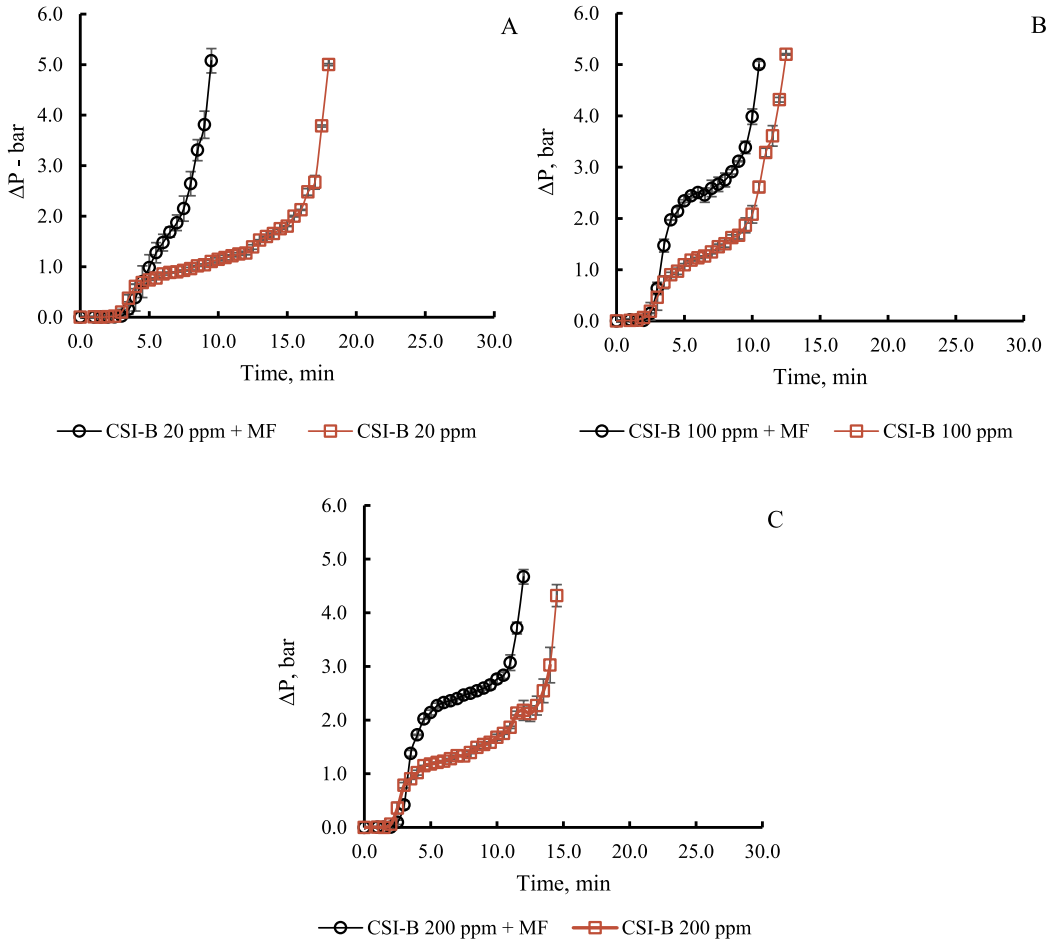

Fig. 6. Changes in pressure (scale formation) as functions of time for calcium and carbonate solutions in the presence of CSI–B at various concentrations following exposure, or not, to an applied magnetic field.

non-inhibitory solutions were analyzed before and after exposure to the MF for comparison.

The majority of scale particles formed in the non-exposed experiments had semi-spherical morphologies with flattened shapes, along with smooth cube-like structures, as shown in Fig. 8-A. These semi-spherical and cubic shapes were identified by XRD as vaterite and calcite, respectively (Fig. 9 and Fig. 10), which is consistent with the results of Ryu et al. (2009) and Flaten et al. (2009), who reported that the morphology of $CaCO_3$ changes into a meta-stable phase when MEG is used as the solvent. In addition, they claimed that higher

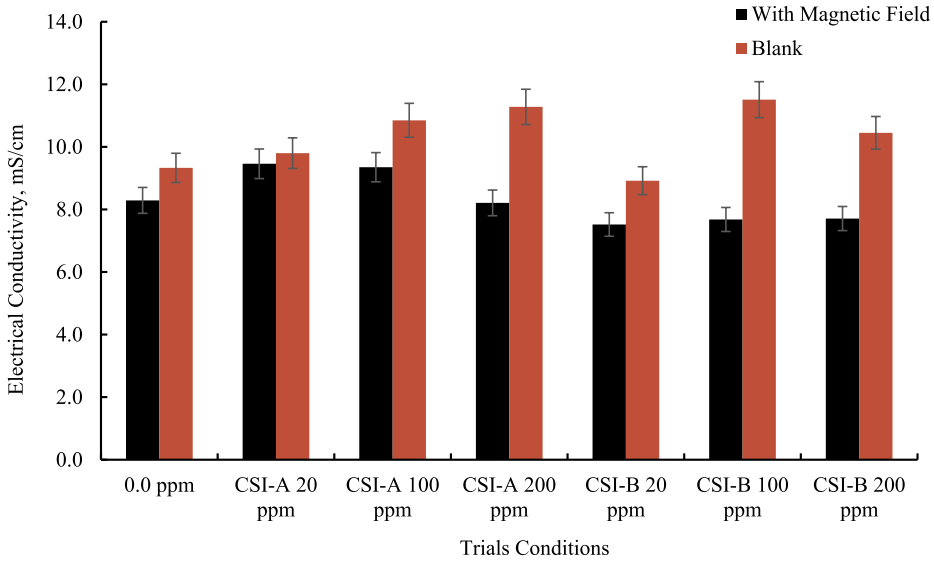

Fig. 7. Electrical conductivities of solutions with various concentrations of CSI-A and CSI–B following exposure, or not, to an applied magnetic field.

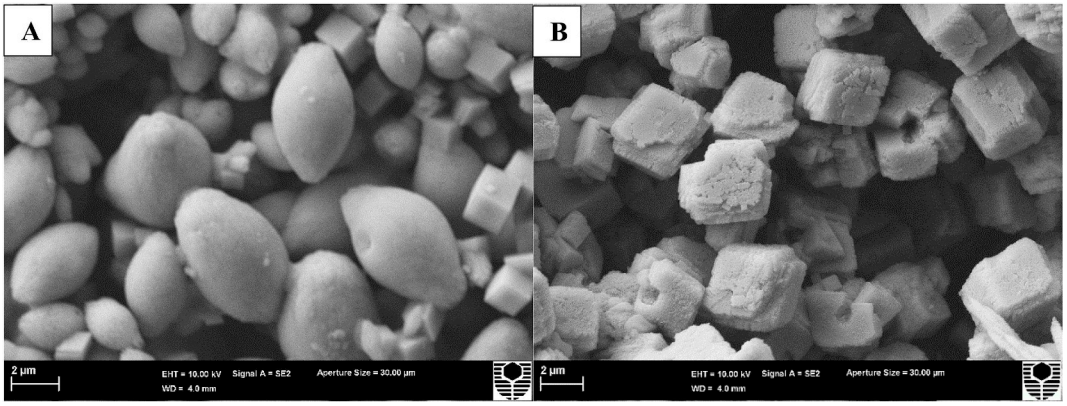

Fig. 8. High-magnification SEM images (scale bar: 2 µm) of scale particles formed under magnetized and non-magnetized conditions in the absence of a CSI: (A) non-magnetized and (B) magnetized.

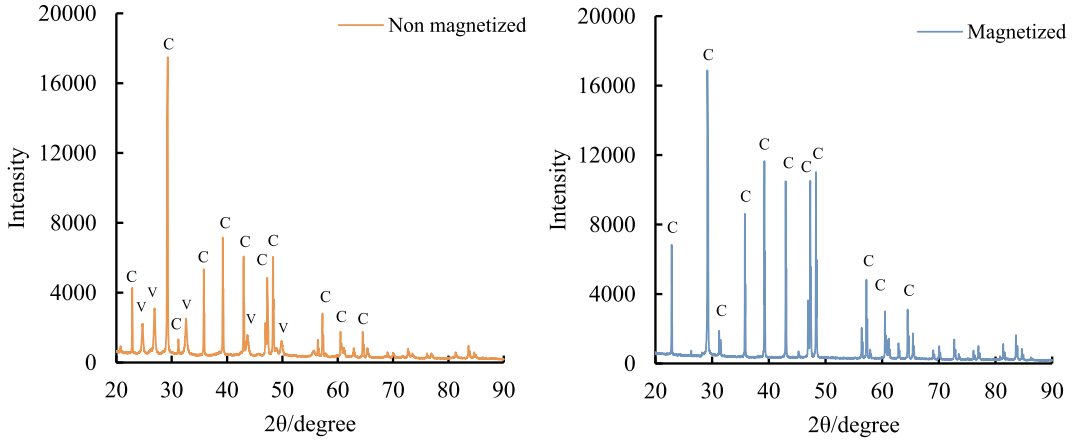

Fig. 9. XRD profiles of (A) vaterite "V" and calcite "C" formed during the non-magnetized experiment, and (B) calcite "C" formed during the magnetized experiment.

temperatures induce the meta-stable morphology in MEG solution. Furthermore, the morphology of $CaCO_3$ is altered at higher initial calcium-ion concentrations and high aqueous glycolic-brine-solution pH (Han et al., 2006). Therefore, we conclude that the $CaCO_3$ morphology is very sensitive to the nature of the solvent, the ion concentration, and the reaction conditions in an aqueous solution.

The geometrical features of the scale particles were seemingly affected by the external MF. Fig. 8-B reveals the formation of cube-like structures with rough surfaces following exposure to the MF at 130 °C; this morphology under these dynamic conditions is unique to this study. Furthermore, the cube-like particles generated in the MF-exposed experiments were larger than those generated in the non-exposed experiments, but slightly smaller than the spherical particles. Unfortunately, the roughened edges of the generated particles led to rapid blockage of the DSL capillary tube, which is consistent with the particle mechanism reported by Saksono et al. (2008). Therefore, the formation of a stable morphology is attributed to the effect of the magnetic field on the thermodynamic conditions during the reactions of calcium and carbonate ions, leading to the generation of more particles with rough cube-like surfaces.

3.5.1. The morphologies of scale formed at different CSI-A concentrations

The formed scale was collected from the outlet solution of the capillary coil after commencement of the experiment and examined by SEM, the results of which are displayed in Fig. 10. The non-exposed sample dosed with 20 ppm CSI-A shows smooth spherical structures along with needle-like and bulk crystalline clusters; the spherical structures were large, distinct, uniform in size, and aggregated. These results demonstrate the effect of MEG and CSI-A on $CaCO_3$ morphology, which results in an apparent deceleration of the rate of precipitate formation. However, after exposure to the external MF, intertwined and interconnected cubic structures were observed; these structures are more likely to accelerate occlusion of the capillary tube because of the small sizes of these deposits that tend to stick to the insides of the pipelines.

As the concentration of CSI-A was increased to 100 ppm in the non-exposed experiment, spherical shapes similar to those observed at the 20-ppm concentration were observed; however, they were smaller and tended to be attracted to each other and overlap, as shown in Fig. 10; this change generated micro-sized crystals that were somewhat differentiated. The crystalline arrangements of the obtained particles reflect the consequences of non-exposed experiments performed at concentrations of 20 and 100 ppm, and differential pressure variations. Accordingly, the time required to block the laboratory capillary tube in both experiments was reasonably close to 12–14 min. Hence, the same morphological form took approximately the same amount of time to block the tubing coil. In contrast, a cube-like morphology was observed after exposure to the MF at 100 ppm CSI-A, which is the same morphology as that observed for experiments performed with 20 ppm CSI-A; however, these cubic particles were less intertwined, and their surfaces were smooth and more distinct.

Increasing the concentration of the CSI-A injected into the brine solution to 200 ppm in the absence of the MF resulted in longitudinal rod-shaped aragonite that formed from smaller groups of longitudinal crystals; SEM revealed that these crystals were ~4.5 µm in size (Fig. 10). The generation of needle-like clusters at a high CSI-A concentration explains the good inhibitory behavior discussed in Section 3.2. We conclude that this concentration of CSI-A inhibitor in glycolic

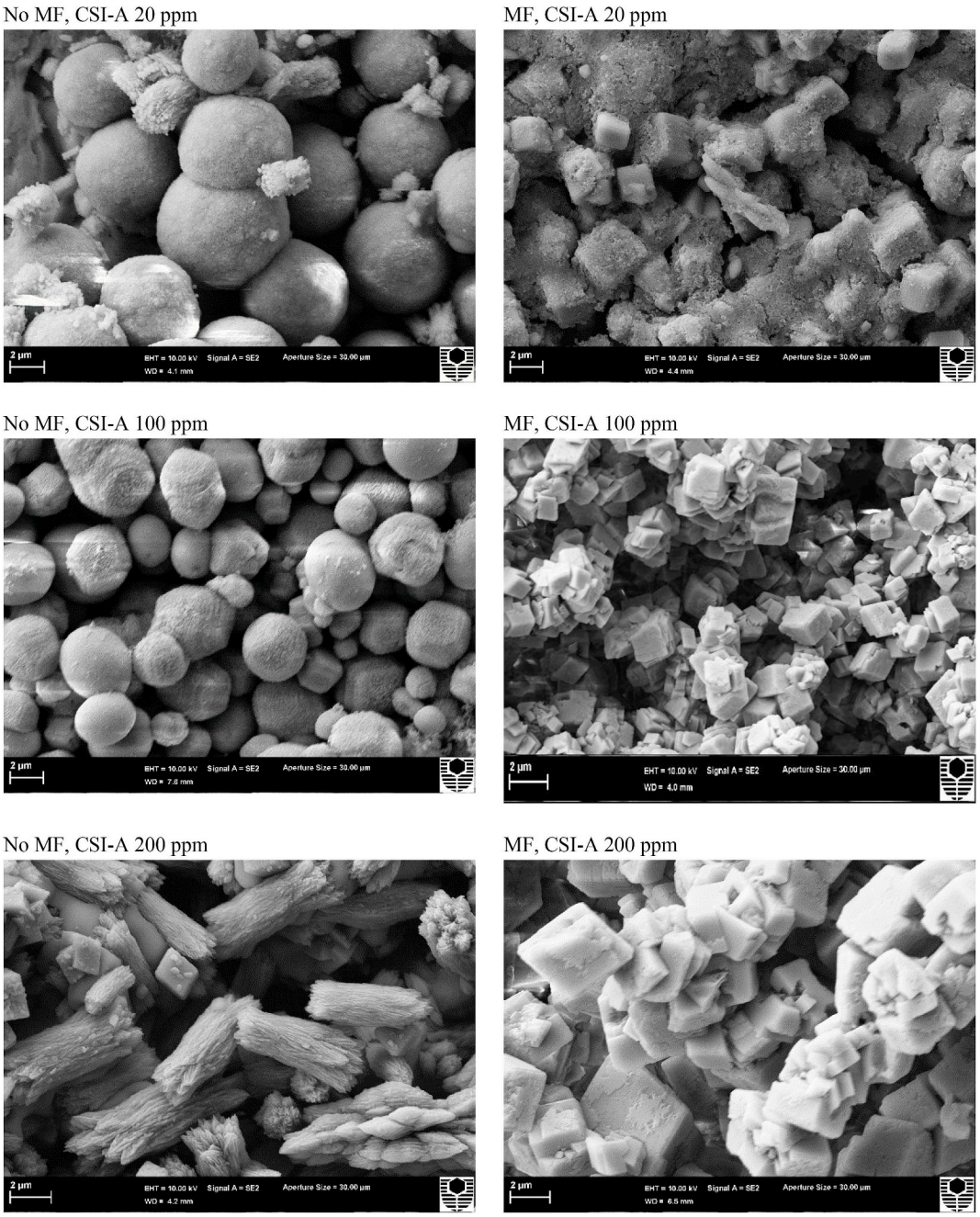

Fig. 10. High-magnification SEM images (scale bar: 2 µm) of scale formed in magnetized and non-magnetized experiments involving CSI-A.

solutions of high concentration, and at a relatively high temperature, reduces the time required to block the flow tubes of high-salinity solutions. However, it is interesting to note that the resulting morphology for the same concentration of CSI-A after exposure to the MF was completely different, and distinctly unintertwined cube-like crystals were formed. Despite this difference in crystallization, the capillary occlusion rates were approximately equal, as described in Sections 3.1–3.3, which is possibly ascribable to the generation of similarly sized crystals with similar nucleation rates due of the same zeta potential values, as discussed in Section 3.7, which promotes cluster formation within the capillary tubes (similar to coagulation or clot formation).

In summary, the glycolic solution affects $CaCO_3$ morphology even in the presence of a CSI. Despite the apparent change in the $CaCO_3$ morphology observed at a CSI-A concentration of 200 ppm, MEG dominated the scale-formation process below 130 °C. Furthermore, these results show that high concentrations of CSI-A alter the morphology of $CaCO_3$ during the inhibition process. Furthermore, in addition to acting as a chelating agent, CSI-A decelerated the rate of $CaCO_3$ formation somewhat. In contrast, scale formation could be reversed by the application of a MF, even after the addition of a CSI.

3.5.2. The morphologies of scale formed at different CSI–B concentrations

The morphologies of the crystals formed before and after exposure to MF at different concentrations of CSI–B were examined in a similar manner to that used in experiments involving CSI-A (Fig. 11). As can be seen, the scale morphologies were very distinct at CSI–B concentrations of 20, 100, and 200 ppm, and exhibited a variety of structures when not exposed to the MF. Cubic and monolithic crystals with rough and distinct surfaces were observed, along with some longitudinal structures that were smaller than these cubic crystals. In contrast, no significant differences were observed in the crystals generated after exposure to the MF; the obtained crystals had cubic and rectangular shapes with

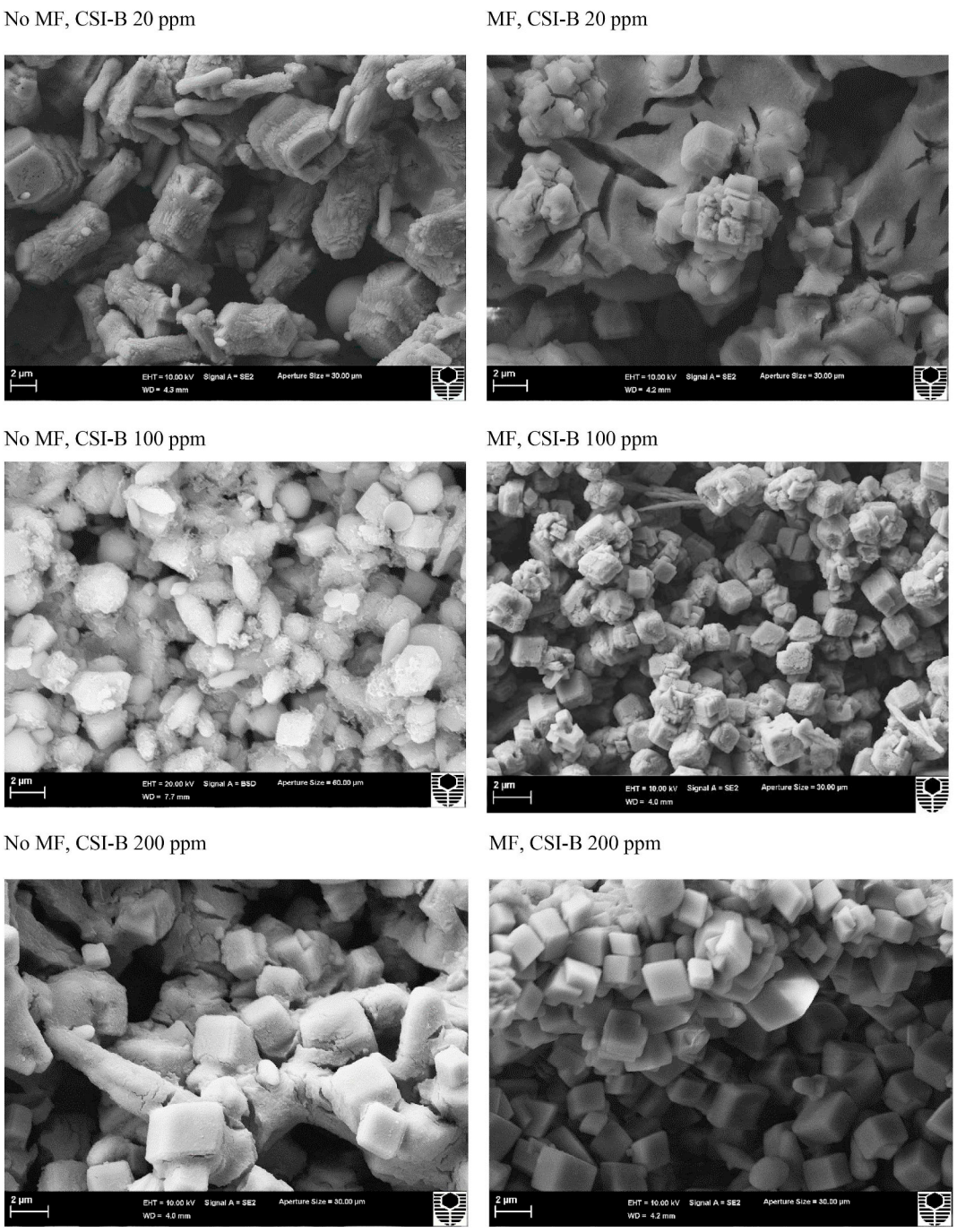

Fig. 11. High-magnification SEM images (scale bar: 2 μm) of scale formed in magnetized and non-magnetized tests of CSI–B.

lower surface roughnesses. In addition, these crystals overlapped to generate a somewhat thick surface. These results indicate that MF treatment created stable $CaCO_3$ morphologies at all CSI–B concentrations. Furthermore, CSI–B failed to inhibit scale formation within the MEG solution at 130 °C, but contributed to the formation of calcium carbonate with a similar, stable phase morphology. These results are unique in that they show that MEG can be prevented from promoting the formation of the meta-stable morphology.

3.6. Particle-size analysis

Particle-size analysis determines the proportion of particles distributed within a colloidal system. Fig. 12 and Fig. 13 compare the particle-size distributions of magnetically treated and non-treated solutions at various scale-inhibitor dosages. Obvious differences in the particle-size distributions were observed between the treated and non-treated samples. The scale particles dispersed in the colloidal system were observed to be more random in size under non-magnetic conditions; this scale also exhibited a wide particles-size distribution. On the other hand, particles 1.0–2.0 μm in size were observed following treatment with CSI-A and CSI–B solutions, at all dosages (Fig. 13). These results show that the magnetized solution induces a significantly smaller particle-size distribution, although the distribution pattern fluctuates with time as larger particles form through aggregation. However, these smaller particles possess higher surface charges and therefore display superior tendencies to stick to hot surfaces or pipe walls, thereby increasing the risk of blockage. On the basis of crystallization theory, the MF also affects crystal nucleation and growth. The

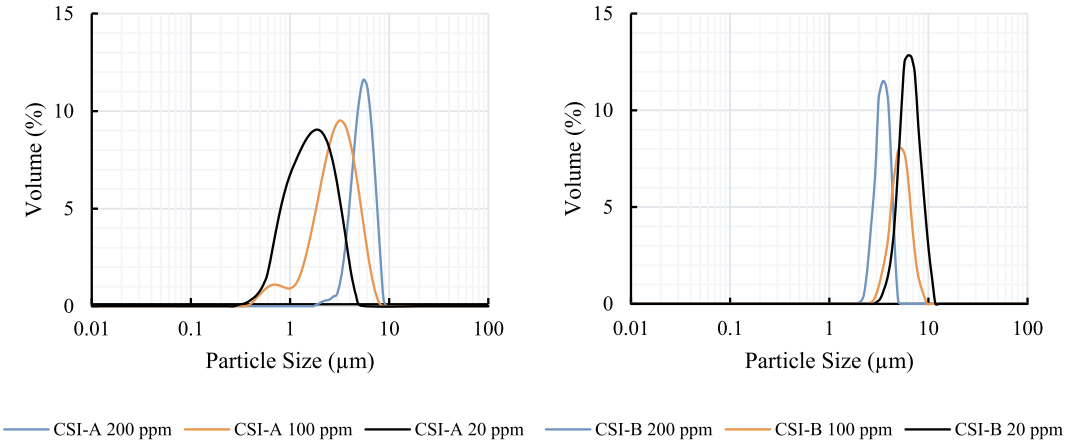

Fig. 12. Particle-size distribution patterns from non-magnetized experiments.

experimental results reveal that a strong magnetic field (0.65 T) and high-energy products can increase the nucleation rate leading to the formation of smaller crystals. These results are particularly interesting as they explain both the crystallization and coagulation mechanism, and reveal that the ζ potential is a quantifiable performance parameter.

3.7. Zeta potential

The zeta potential (ζ) provides an indication of interactions between particles and is an essential aggregate-forming factor. The measured zeta potentials were negative in all experiments because of the high operating pH values. Consequently, the absolute values of the measured zeta potentials were adopted in this study. Fig. 14 compares the absolute ζ values of the magnetized (ζ_m) and non-magnetized (ζ_u) solutions as functions of CSI concentration for samples containing 80 vol% MEG, with the values tabulated in Table 4. Furthermore, the results from exposed and non-exposed blank (no CSI) experiments are also included in Fig. 14. The ζ_m values for the magnetized MEG-brine solutions were always found to be lower in magnitude than those ζ_u of the non-magnetized solutions indicating a greater potential for particle agglomeration and hence scale formation.

The ratio between corresponding magnetized and non-magnetized zeta potentials ($1-\zeta_m/\zeta_u$) is also reported in Table 4 to further illustrate the reduced effect of MF exposure with increasing CSI concentration. As the concentration of the CSI increased, the MF appeared to have a reduced effect on the formed particles zeta potential almost reaching parity at 200 ppm CSI dosage rate. The reduced effect of MF as CSI concentration increased is in line with the experimental DSL results where the difference in scale formation rate between magnetized and non-magnetized experiments also decreased. Ultimately, this result may indicate that in the higher CSI concentration tests, the effect of CSIs on the scale formation is dominant over the potential effect of the MF.

Higashitani et al. (1995) reported that well-mixed solutions composed of colloids and electrolytes exposed to a MF exhibited lower ζ values than the same solutions that were not exposed to the MF, which is consistent with the results obtained in this study. Furthermore (Parsons et al., 1997), and Alabi et al. (2015) concluded that a MF does affect colloidal stability, thereby modifying the charge density in the vicinity of the Stern layer. Also, synergism between the high magnetic energy produced and the high pH within the glycolic solution may appropriately explain the observed decrease in absolute ζ value when an external MF is applied. Ellingsen and Kristiansen (1979) reported that MF treatment is affected by solution pH as $CaCO_3$ precipitation is inhibited at pH greater than 9.3 and enhanced at pH below 9.0. Hence, the operating pH in this study explains the reduction in ζ potential under MF conditions. The differences in the transmission rates of ions in the medium and altered double-layer properties of the glycolic environment also affected the ζ value (Fig. 15); hence, the interaction rates for the formation of scale before and after exposure to MF were different. In addition, magnetic treatment promotes the susceptibilities of the molecules in the suspension to coagulate by decreasing double-layer repulsion, which results in a reduction in particle surface area. This facilitates the penetration of ions into the liquid phase, which leads to a reduction in the density of the diffuse layer and a proportional reduction in the surface charge. This proposal is consistent with the reports of Krylov et al. (1985) and Parsons et al. (1997). Furthermore,

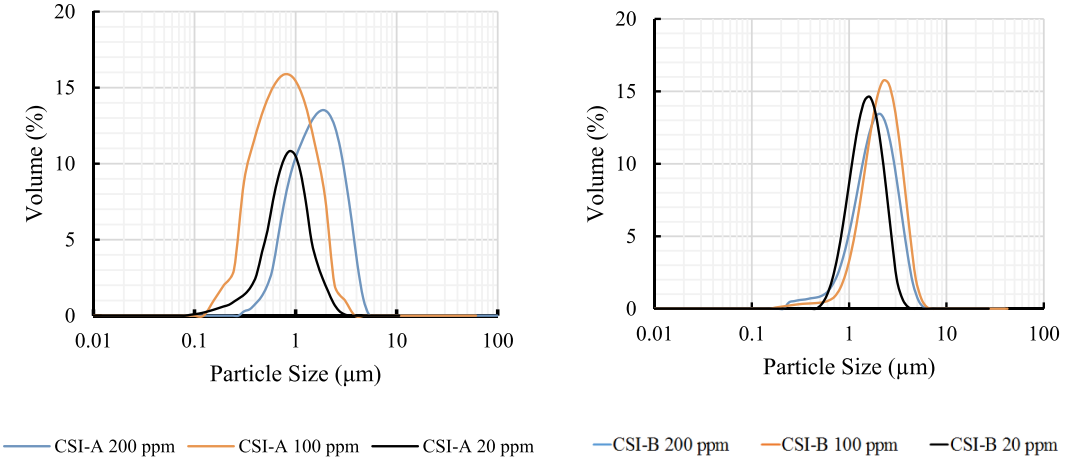

Fig. 13. Particle-size distribution patterns from magnetized experiments.

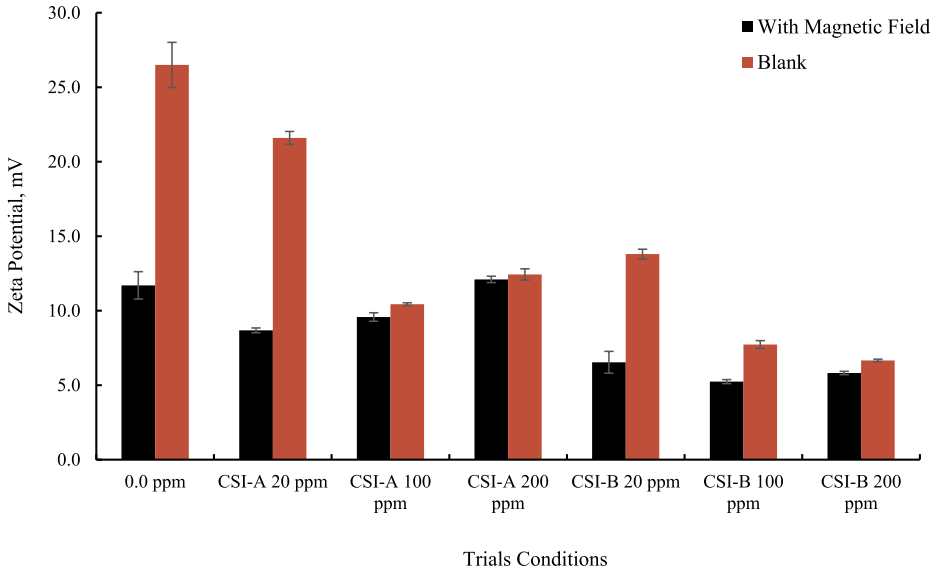

Fig. 14. Absolute zeta potentials of solutions with various CSI-A and CSI–B concentrations following exposure, or not, to an applied magnetic field.

Table 4
Absolute zeta potentials of magnetized and non-magnetized solutions with various CSI concentrations.

CSI and Dosage	ζ_m	ζ_u	$(1 - \zeta_m/\zeta_u)$
0.0 ppm	11.70	26.50	0.56
CSI-A 20 ppm	8.68	21.60	0.60
CSI-A 100 ppm	9.58	10.43	0.09
CSI-A 200 ppm	12.10	12.43	0.03
CSI–B 20 ppm	6.54	13.80	0.53
CSI–B 100 ppm	5.24	7.73	0.33
CSI–B 200 ppm	5.82	6.66	0.13

occlusion in the capillary coil, as discussed in Sections 3.1–3.3, is a result of changes in the $CaCO_3$ morphology resulting from exposure to the MF. These changes lead to the formation of deposits with stable morphologies that accelerated blockage of the conveyor tubes because of the small ζ values resulting from the applied MF. These results are consistent with the findings of Higashitani et al. (1993), who reported that although the nucleation of calcium carbonate was delayed, its growth was accelerated by high external magnetic-flux density. Hence, the presence of MEG and mineral ions altered the electro-kinetic potential in the ionic-dispersion system when the MF was applied.

The accelerated scale formation can be also described by the spin-chemistry mechanism, in which a weak internal magnetic field is generated by the electron spin within an atomic orbital (Scott, 2012; Steiner and Ulrich, 1989; Chibowski and Szcześ, 2018). This weak internal magnetic field manages the reactions of calcium and bicarbonate ions leading to increased scale formation in the presence of a powerful external magnetic effect (Steiner and Ulrich, 1989; Chibowski and Szcześ, 2018). This promotion is attributed to the ability of the magnetic field to accelerate the forward reaction by decreasing the frequency of the reverse reaction. In other words, the magnetic field prevents the products from returning back to their original states (Till and Hore, 1997; Timmel et al., 1998). This result is consistent with the radical-pair mechanism in the presence of an external magnetic field as reported in several publications (Scott, 2012; Steiner and Ulrich, 1989; Chibowski and Szcześ, 2018). Therefore, the effects of magnetic fields on scale-formation reactions can be described by spin-chemistry theory.

3.8. Effect of magnetic field on individual parameters

3.8.1. Ionic hydration shell

Mineral ions tend to interact with water or solvent molecules to form encapsulating hydration or solvation shells (BURGOS-Cara et al., 2017), whose thicknesses vary according to the thermodynamic

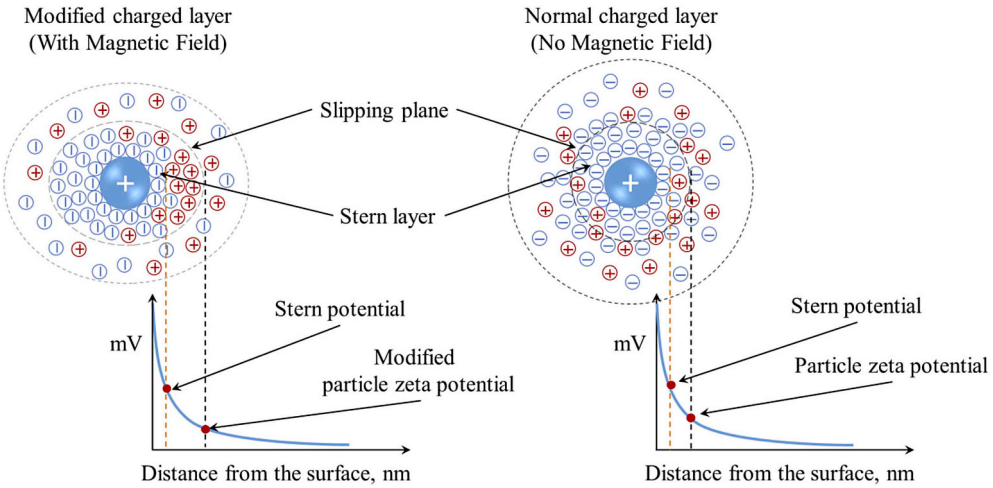

Fig. 15. Depicting a possible mechanism for the effect of a magnetic field based on zeta-potential difference (Alabi et al., 2015).

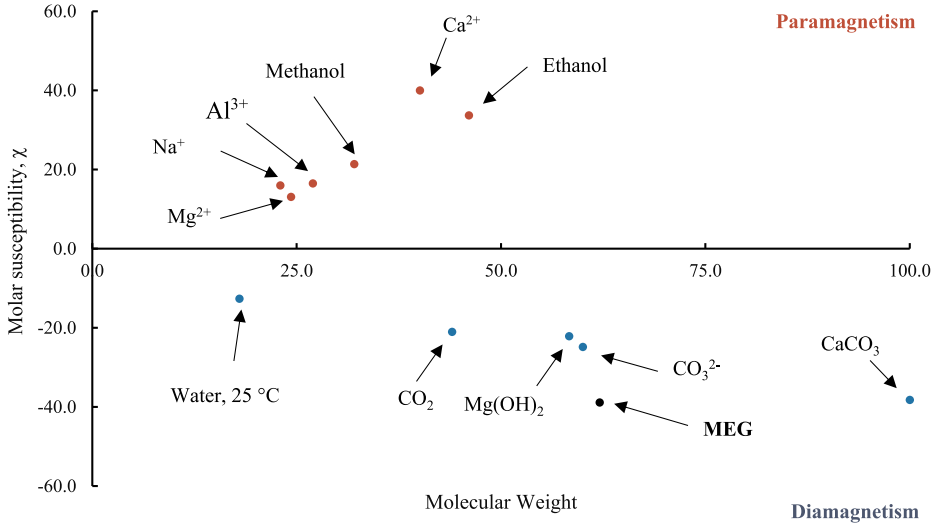

Fig. 16. Molar susceptibilities of elements at room temperature (cgs units of 10^{-6} cm^3/mol)(Lide, 2009).

conditions (Moosavi and Gholizadeh, 2014). Furthermore, it has been reported that EC and hydration-shell thickness are inversely related (Holysz et al., 2007). Therefore, observed reductions in EC values are attributable to the weak bonding of ions with water molecules that increase the thicknesses of their solvation shells. Furthermore, exposure to the MF contributes to a lower ζ value that changes the thickness of the slipping-plane layers of the particles, which also lowers the EC value as described by the Henry Equation (see Equation (1)). These results are consistent with those of previously published reports, in which similar relationships between the hydration shell and zeta potential were observed (Lv et al., 2014; Chibowski and Szcześ, 2018). Therefore, the closed-loop relationship between the hydration shell, EC, and ζ provides a theoretical explanation for the effects of MFs on saline solutions (see Equation (2)). An increase in ζ value is usually an indication of repulsion between molecules; the higher the ζ value, the greater the repulsion, which leads to a reduced coagulation rate (Ding and Keh, 2001). However, the thermodynamic and electro-kinetic conditions alter upon exposure to a MF, leading to different ζ and electrophoretic-mobility values and hydration-shell thicknesses.

$$\zeta = \frac{\varepsilon . u}{\mu} f(k . R_s), \quad 1$$

where, u_m denotes electrophoretic mobility, ε is the dielectric constant, μ is the viscosity, k is the Debye–Hückel parameter, and R_s is the particle radius (Kaszuba et al., 2010). Electrophoretic mobility and ionic conductivity (σ) can be also calculated by Stokes' law and the force fields associated with the ion at drift velocity, and Nernst-Einstein as shown by the following equations (Higashitani and Oshitani, 1998; Luo and Nguyen, 2017; Gouverneur et al., 2015; Harris, 2010; Matvejev et al., 2012):

$$u_m = \frac{e . z}{6 . \pi . \mu . r} = \frac{e . z . D}{k_B . T}, \quad 2$$

$$\sigma = \frac{(e . z)^2 c . D}{k_B . T}, \quad 3$$

Combining Equations (2) and (3) leads to the following relationship:

$$\sigma = e . z . c . u_m, \quad 4$$

where, e denotes the elementary charge, z is the number of ionic charges, r is the hydrodynamic radius including water ligands, D is the diffusion coefficient, k_B is the Boltzmann constant, T is the temperature, and c is the volume concentration of the ions.

The thermodynamic conditions also change in the presence of a CSI, high alkalinity, and other organic additives such as MEG. Such changes can lead to different results for ionic water binding systems exposed to a MF. In all experiments carried out in this study, we observed that the MF contributed to the accelerated blockage of laboratory capillary coils, even when a CSI was used. This acceleration was due to the presence of high concentrations of MEG that increase the viscosity of the solution and reduce the solubilities of the mineral ions, as well as pH values above 9.3 (Ellingsen and Kristiansen, 1979). It is well-known that MEG molecules form hydrogen bonds with water molecules, thereby altering the thermodynamic behavior of water molecules toward bonding with dissolved ions and the formation of hydration shells (Rozhkova et al., 2007). In addition, previous reports have indicated that MEG molecules directly decrease the saturation and ionizing levels of species in aqueous solutions, rendering the formation of inorganic scale more likely (Shen et al., 2008; Montazaud, 2011). These thermodynamic conditions, when combined with MF treatment, promote the formation of mineral deposits in the presence of a CSI.

3.8.2. Molecular susceptibilities

Magnetic susceptibility is a critical factor that determines the responses of ions and molecules to external MFs (Chibowski and Szcześ, 2018). MEG, water, and carbonate ions are diamagnetic substances; i.e., they are repelled by magnets in a temperature-independent manner (Lide, 2009; Silberberg, 2006). However, the magnetic susceptibility of water is reportedly three times lower than that of MEG and two times lower than that of carbonate ions (Lide, 2009). Therefore, the magnetizations (M) of molecular MEG and CO_3^{2-} are much stronger than that of water, as indicated by the following equation:

$$M_i = \chi_m . V_m . \overrightarrow{H_i}, \quad 5$$

where, χ_m is the molar susceptibility ($\times 10^{-6}$ cm^3 mol^{-1}), V_m is the molar volume, and $\overrightarrow{H_i}$ is the magnetic-field strength (Lide, 2009). In contrast, calcium ions are known to be paramagnetic and consequently interact with an external MF (see Fig. 16) (Lide, 2009; Silberberg, 2006). Therefore, calcium and carbonate ions can be separated from water molecules in aqueous solutions, as shown in Fig. 17. This separation inhibits scale formation after exposure to the MF. However, the molecular arrangements of MEG and water are modified by the MF (Sandengen, 2006); the MEG molecules are expected to be located away from both the calcium and carbonate ions, leading to increased supersaturation; in other words, both ions are more likely to interact with each, particularly when the concentration of water molecules is reduced by increasing the amount of MEG present (Flaten et al., 2015; Sandengen, 2006). Therefore, the formed ion hydration shell remains the determining factor that inhibits or promotes scale formation (AL

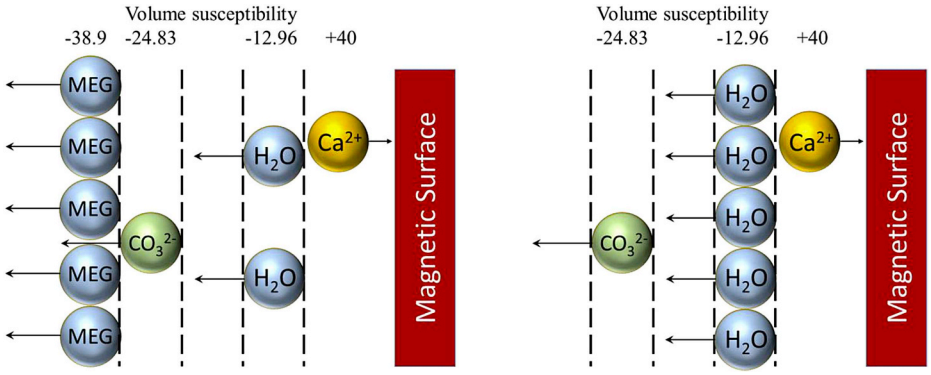

Fig. 17. Magnetic volume susceptibilities of admixtures of substances in MEG and water systems after exposure to a magnetic field.

Helal et al., 2018; Silva et al., 2015).

4. Conclusion

This study was undertaken to study the effect of magnetic fields on the performance of chemical scale inhibitors within MEG solutions. Prior studies have shown that the application of magnetic field treatment can inhibit the formation of mineral-ion scale in both water and rich MEG systems (AL Helal et al., 2018; AL Helal et al., 2019), however, the combined effect of MFs with CSIs is uncertain. With this in mind, two commercially available CSIs were examined in the presence of a 0.650-T external MF field under conditions potentially found within an industrial MEG regeneration system reboiler (130 °C, pH 9.5). Overall, the results showed that inorganic deposits such as $CaCO_3$ form more rapidly within high MEG concentration solution when exposed to a MF under the conditions tested. The accelerated rate of deposit formation due to the applied MF, also negatively affected the performance of the chemical inhibitors used in this study, irrespective of their concentrations. The application of the MF resulted in several key effects on the scale formation process including:

- Exposure to the MF produced a stable calcium carbonate (calcite) phase morphology, even when CSIs were used.
- Exposure to the MF resulted generated small sized particles compared to those of non-magnetized solutions in the presence of the CSIs.
- The absolute zeta potential of particles formed in the presence of the applied MF and MEG was lower than that in the absence of the MF. The relationship between the thickness of the hydration shell and the EC value is consistent with previously reported results for MF exposure.
- The results indicate that the effect of the applied magnetic field is retained even after heating the solution to high temperatures, a result contrary the findings of Silva et al. (2015).

The findings summarized above are significant in terms of understanding the effect of an applied MF on scale formation. The most significant finding was the apparent differences in ζ potential values. Although the measured values were not particularly high, the consistently observed differences in ζ potential before and after exposure to the MF highlight the ability of the MF to change the external charges on the surfaces of molecules present in solution, thereby changing the thicknesses of the hydration shells that encapsulates these ions. These results provide significant insight into the effect of a MF on scale formation, irrespective of whether or not a CSI is used, and helps to interpret the effects of various treatments for scale removal or the prevention of scale formation. Investigations into the abilities of MFs to fundamentally change scale formation during various operations including the MEG regeneration process are still in their early stages and require further intensive study.

Although it was consistently observed that application of a MF ultimately increased the rate of scale formation, something undesirable in most industrial operations, the application of MF treatment may have potential benefits during the MEG regeneration process. In some MEG systems, pre-treatment is performed in order to removal divalent cationic species that would otherwise scale and foul the down-stream regeneration column operating at high temperature (Alharooni et al., 2017; Brustad et al., 2005; Soames et al., 2019). The application of a MF inside the pre-treatment system may promote the formation of divalent salt products even in the presence of CSIs, allowing their separation and removal in down-stream precipitation vessels before entering the regeneration system. Overall, this study provides a reasonable assessment of the effects of the various treatments employed for preventing scale formation or scale removal in the reboiler section during the MEG regeneration process.

Acknowledgments

We would like to express our sincere gratitude to the Curtin Corrosion Engineering Industry Centre (CCEIC), the W.A. School of Mines: Minerals, Energy and Chemical Engineering at Curtin University and the Al-Khwarizmi College of Engineering at Bicol University for their support for this study. Furthermore, the authors would like to thank Dr. Franca Jones for her continued support of this work. Part of this research was undertaken using the EM/XRD/SAXS/XPS instrumentation (Australian Research Council grant number LE0775553) at the John de Laeter Centre, Curtin University.

Appendix A. Supplementary data

Supplementary data to this article can be found online at https://doi.org/10.1016/j.petrol.2019.04.093.

References

AL Helal, A., Soames, A., Gubner, R., Iglauer, S., Barifcani, A., 2018. Influence of magnetic fields on calcium carbonate scaling in aqueous solutions at 150° C and 1 bar. J. Colloid Interface Sci. 509, 472–484.
AL Helal, A., Soames, A., Iglauer, S., Gubner, R., Barifcani, A., 2019. The influence of magnetic fields on calcium carbonate scale formation within monoethylene glycol solutions at regeneration conditions. J. Pet. Sci. Eng. 173, 158–169.
Alabi, A., Chiesa, M., Garlisi, C., Palmisano, G., 2015. Advances in anti-scale magnetic water treatment. Environ. Sci.: Water Res. Technol. 1, 408–425.
Alharooni, K., Gubner, R., Iglauer, S., Pack, D., Barifcani, A., 2017. Influence of regenerated monoethylene glycol on natural gas hydrate formation. Energy Fuels 31, 12914–12931.
Amiri, M., Moghadasi, J., Jamialahmadi, M., Shahri, M.P., 2013. The study of calcium sulfate scale formation during water injection in Iranian oil fields at different pressures. Energy Sources, Part A Recovery, Util. Environ. Eff. 35, 648–658.
Amjad, Z., 2010. The Science and Technology of Industrial Water Treatment. CRC Press.
Amjad, Z., 2013. Mineral Scales in Biological and Industrial Systems. CRC Press.
Amjad, Z., Albright, J., 2015. Kinetic and Morphological Investigation of Strontium Sulfate Precipitation in the Presence of Biopolymers and Synthetic Polymers for Oilfield Applications. CORROSION 2015. NACE International.

Babu, D., Hosseinzadeh, M., Ehsaninejad, A., Babaei, R., Kashkooli, M., Akbary, H., 2015. Carbonates precipitation in MEG loops–A comparative study of South Pars and Bass Strait gas fields. J. Nat. Gas Sci. Eng. 27, 955–966.
Bader, M., 2006. Sulfate scale problems in oil fields water injection operations. Desalination 201, 100–105.
BARAKA-Lokmane, S., Hurtevent, C., Ohanessian, J.-L., Rousseau, G., Seiersten, M.E., Deshmush, S., 2012. Prediction of mineral scaling in a MEG loop system of a gas production offshore. In: SPE International Conference on Oilfield Scale. Society of Petroleum Engineers.
Brustad, S., Løken, K.-P., Waalmann, J.G., 2005. Hydrate Prevention using MEG instead of MeOH: impact of experience from major Norwegian developments on technology selection for injection and recovery of MEG. In: Offshore Technology Conference, (Offshore Technology Conference).
BURGOS-Cara, A., Putnis, C.V., RODRIGUEZ-Navarro, C., RUIZ-Agudo, E., 2017. Hydration effects on the stability of calcium carbonate pre-nucleation species. Minerals 7, 126.
Cavano, R.R., 2005Cavano,. Understanding scaling indices and calculating inhibitor dosages. In: CORROSION 2005. NACE International.
Chang, M.-C., Tai, C.Y., 2010. Effect of the magnetic field on the growth rate of aragonite and the precipitation of CaCO 3. Chem. Eng. J. 164, 1–9.
Chang, K.-T., Weng, C.-I., 2006. The effect of an external magnetic field on the structure of liquid water using molecular dynamics simulation. J. Appl. Phys. 100 043917.
Chibowski, E., Szcześ, A., 2018. Magnetic water treatment–A review of the latest approaches. Chemosphere 203, 54–67.
Cole, K., 2015. An Experimental Comparison of Three Scale Control Materials. University of Louisiana at Lafayette.
Daniels, J.K., Littlehales, I., Lau, L., LINARES-Samaniego, S., 2014. Laboratory methods for scale inhibitor selection for HP/HT fields. In: SPE International Oilfield Scale Conference and Exhibition. Society of Petroleum Engineers, Aberdeen, Scotland.
Dhanaraj, G., Byrappa, K., Prasad, V., Dudley, M., 2010. Springer Handbook of Crystal Growth. Springer Science & Business Media.
Ding, J.M., Keh, H.J., 2001. The electrophoretic mobility and electric conductivity of a concentrated suspension of colloidal spheres with arbitrary double-layer thickness. J. Colloid Interface Sci. 236, 180–193.
Ellingsen, F., Kristiansen, H., 1979. Does magnetic treatment influence precipitation of calcium carbonate from supersaturated solutions. Vatten 35, 309–315.
Esmaeilnezhad, E., Choi, H.J., Schaffie, M., Gholizadeh, M., Ranjbar, M., 2017. Characteristics and applications of magnetized water as a green technology. J. Clean. Prod. 161, 908–921.
Fan, C., Shi, W., Zhang, P., Lu, H., Zhang, N., Work, S., AL-Saiari, H., Kan, A., Tomson, M., 2012. Ultrahigh-temperature/ultrahigh-pressure scale control for deepwater oil and gas production. SPE J. 17, 177–186.
Flaten, E.M., Ma, X., Seiersten, M., Aanonsen, C., Beck, R., Andreassen, J.-P., 2015. Impact of Monoethylene Glycol and Fe2+ on Crystal Growth of CaCO3. CORROSION 2015. NACE International.
Flaten, E.M., Seiersten, M., Andreassen, J.-P., 2009. Polymorphism and morphology of calcium carbonate precipitated in mixed solvents of ethylene glycol and water. J. Cryst. Growth 311, 3533–3538.
Gouverneur, M., Kopp, J., van Wullen, L., Schonhoff, M., 2015. Direct determination of ionic transference numbers in ionic liquids by electrophoretic NMR. Phys. Chem. Chem. Phys. 17, 30680–30686.
Graham, G., Gyani, A., Jordan, M., Strachan, C., Mcclure, R., Littlehales, I., Fitzgerald, A., 2002. Selection and application of a non-damaging scale inhibitor package for preemptive squeeze in mungo production wells. In: International Symposium on Oilfield Scale. Society of Petroleum Engineers.
Guan, H., 2015. Scale Deposition Control and Management in Subsea Fields. NACE International.
Halvorsen, A.M.K., Andersen, T.R., Halvorsen, E.N., Kojen, G.P., Skar, J.I., Biørnstad, C., Fitje, H., 2007. The relationship between internal corrosion control method, scale control and meg handling of a multiphase carbon steel pipeline carrying wet gas with CO2 and cetic acid. In: CORROSION 2007. NACE International, Nashville, Tennessee.
Han, Y.S., Hadiko, G., Fuji, M., Takahashi, M., 2006. Factors affecting the phase and morphology of CaCO3 prepared by a bubbling method. J. Eur. Ceram. Soc. 26, 843–847.
Harris, D.C., 2010. Quantitative Chemical Analysis. Macmillan.
Higashitani, K., Oshitani, J., 1998. Magnetic effects on thickness of adsorbed layer in aqueous solutions evaluated directly by atomic force microscope. J. Colloid Interface Sci. 204, 363–368.
Higashitani, K., Kage, A., Katamura, S., Imai, K., Hatade, S., 1993. Effects of a magnetic field on the formation of CaCO3 particles. J. Colloid Interface Sci. 156, 90–95.
Higashitani, K., Iseri, H., Okuhara, K., Kage, A., Hatade, S., 1995. Magnetic effects on zeta potential and diffusivity of nonmagnetic colloidal particles. J. Colloid Interface Sci. 172, 383–388.
Holysz, L., Szczes, A., Chibowski, E., 2007. Effects of a static magnetic field on water and electrolyte solutions. J. Colloid Interface Sci. 316, 996–1002.
Hyllestad, K., 2013. Scaling of Calcium Carbonate on a Heated Surface in a Flow through System with Mono Ethylene Glycol. Norwegian University of Science and Technology.
Kaasa, B., Sandengen, K., Ostvold, T., 2005. Thermodynamic predictions of scale potential, pH and gas solubility in glycol containing systems. In: SPE International Symposium on Oilfield Scale. Society of Petroleum Engineers.
Kan, A.T., Fu, G., Watson, M.A., Tomson, M.B., 2002. Effect of hydrate inhibitors on oilfield scale formation and inhibition. In: International Symposium on Oilfield Scale. Society of Petroleum Engineers.
Kan, A., Wu, X., Fu, G., Tomson, M., 2005. Validation of scale prediction Algorithms at oilfield conditions. In: SPE International Symposium on Oilfield Chemistry. Society of Petroleum Engineers.
Kaszuba, M., Corbett, J., Watson, F.M., Jones, A., 2010. High-concentration zeta potential measurements using light-scattering techniques. Phil. Trans. Roy. Soc. Lond.: Math. Phys. Eng. Sci. 368, 4439–4451.
Kochmarsky, V., 1996. Magnetic treatment of water: possible mechanisms and conditions for applications. Phys. Separ. Sci. Eng. 7, 77–107.
Krylov, O., Vikulova, I., Eletskii, V., Rozno, N., Klassen, V., 1985. Influence of magnetic treatment on the electrokinetic properties of a suspension of calcium carbonate. Coll. J. Ussr 47, 31–38.
Lide, D.R., 2009. CRC Handbook of Chemistry and Physics: a Ready-Reference Book of Chemical and Physical Data, Boca Raton, Fla. London, Boca Raton, Fla. CRC, London.
Lu, H., Kan, A.T., Tomson, M.B., 2010. Effects of monoethylene glycol on carbonate equilibrium and calcite solubility in gas/monoethylene glycol/NaCl/water mixed systems. SPE J. 15, 714–725.
Luo, L., Nguyen, A.V., 2017. A review of principles and applications of magnetic flocculation to separate ultrafine magnetic particles. Separ. Purif. Technol. 172, 85–99.
Lv, W., Feng, J., Yan, W., Faul, C.F., 2014. Self-assembly and pH response of electroactive liquid core–tetra (aniline) shell microcapsules. J. Mater. Chem. B 2, 4720–4725.
Matvejev, V., Zizi, M., Stiens, J., 2012. Hydration shell parameters of aqueous alcohols: THz excess absorption and packing density. J. Phys. Chem. B 116, 14071–14077.
Messiha, H.L., Wongnate, T., Chaiyen, P., Jones, A.R., Scrutton, N.S., 2015. Magnetic field effects as a result of the radical pair mechanism are unlikely in redox enzymes. J. R. Soc. Interface 12, 20141155.
Montazaud, T., 2011. Precipitation of Carbonates in the Pretreatment Process for Regeneration of Ethylene Glycol. Norwegian University of Science and Technology.
Moosavi, F., Gholizadeh, M., 2014. Magnetic effects on the solvent properties investigated by molecular dynamics simulation. J. Magn. Magn. Mater. 354, 239–247.
NACE International, N., 2005. Dynamic Scale Inhibitor Evaluation Apparatus and Procedures in Oil and Gas Production. NACE International.
NACE International, N., 2016. Laboratory Screening Tests to Determine the Ability of Scale Inhibitors to Prevent the Precipitation of Calcium Sulfate and Calcium Carbonate from Solution (For Oil and Gas Production Systems). NACE International.
NSTM0374, N.S., 2007. Laboratory Screening Tests to Determine the Ability of Scale Inhibitors to Prevent the Precipitation of Calcium Sulfate and Calcium Carbonate from Solution (For Oil and Gas Production Systems). National Association of Corrosion Engineers.
Østvold, T., Randhol, P., 2001. Kinetics of CaCO3 scale formation. The influence of temperature, supersaturation and ionic composition. In: International Symposium on Oilfield Scale. Society of Petroleum Engineers.
Parsons, S.A., Wang, B.-L., Judd, S.J., Stephenson, T., 1997. Magnetic treatment of calcium carbonate scale—effect of pH control. Water Res. 31, 339–342.
Perez, L.A., Amjad, Z., Zuhl, R.W., 2016. Stressed Cooling Water System Deposit Control Management. NACE International, CORROSION.
Racke, K.D., 1992. Degradation of Organophosphorus Insecticides in Environmental Matrices. Organophosphates Chemistry, Fate, and Effects. Elsevier.
Rajczykowski, K., Loska, K., 2018. Stimulation of heavy metal adsorption process by using a strong magnetic field. Water, Air, Soil Pollut. 229, 20.
Ramzia, M., R.H., El-Sayedb*, M., Fathyc, M., Moghnyc, T.A., 2016. Evaluation of scale inhibitors performance under simulated flowing field conditions using dynamic tube blocking test. Int. J. Chem. Sci. 14, 16–28.
Rodgers, C.T., 2009. Magnetic field effects in chemical systems. Pure Appl. Chem. 81, 19–43.
Rozhkova, M., Rozhkova, A., Butyrskaya, E., 2007. Separation of mineral salts and nonelectrolytes (ethylene glycol) by dialysis through ion-exchange membranes. J. Anal. Chem. 62, 710–715.
Ryu, M., Ahn, J., You, K., Goto, S., Kim, H., 2009. Synthesis of calcium carbonate in ethanol-ethylene glycol solvent. J. Ceram. Soc. Jpn. 117, 106–110.
Saksono, N., Gozan, M., Bismo, S., Krisanti, E., Widaningrum, R., Song, S.K., 2008. Effects of magnetic field on calcium carbonate precipitation: ionic and particle mechanisms. Kor. J. Chem. Eng. 25, 1145–1150.
Sandengen, K., 2006. Prediction of Mineral Scale Formation in Wet Gas Condensate Pipelines and in MEG (Mono Ethylene Glycol) Regeneration Plants. Norwegian University of Science and Technology.
Scott, L., 2012. Reduced Calcium Carbonate Scaling through Turbulent Physical Conditioning.
Shen, D., Fu, G., Alsaiari, H.A., Kan, A.T., Tomson, M.B., 2008. Seawater injection, inhibitor transport and rock-brine interactions. In: SPE International Oilfield Scale Conference. Society of Petroleum Engineers.
Silberberg, M.S., 2006. Chemistry : the Molecular Nature of Matter and Change/Martin S. Silberberg. McGraw-Hill, Boston, Boston.
Silva, I.B., Neto, J.C.Q., Petri, D.F., 2015. The effect of magnetic field on ion hydration and sulfate scale formation. Colloid. Surf. Physicochem. Eng. Asp. 465, 175–183.
Soames, A., Odeigah, E., AL Helal, A., Zaboon, S., Iglauer, S., Barifcani, A., Gubner, R., 2018. Operation of a MEG pilot regeneration system for organic acid and alkalinity removal during MDEA to FFCI switchover. J. Pet. Sci. Eng. 169, 1–14.
Soames, A., Barifcani, A., Gubner, R., 2019. Removal of Organic Acids during Monoethylene Glycol Distillation and Reclamation to Minimize Long-Term Accumulation. (Book review).
Sorbie, K., Laing, N., 2004. How scale inhibitors work: mechanisms of selected barium sulphate scale inhibitors across a wide temperature range. In: SPE International Symposium on Oilfield Scale. Society of Petroleum Engineers.
Steiner, U.E., Ulrich, T., 1989. Magnetic field effects in chemical kinetics and related phenomena. Chem. Rev. 89, 51–147.
Szczes, A., Chibowski, E., Holysz, L., Rafalski, P., 2011. Effects of static magnetic field on electrolyte solutions under kinetic condition. J. Phys. Chem. A 115, 5449–5452.
Tai, C.Y., Wu, C.-K., Chang, M.-C., 2008. Effects of magnetic field on the crystallization of

CaCO 3 using permanent magnets. Chem. Eng. Sci. 63, 5606–5612.
Tai, C.Y., Chang, M.-C., Yeh, S.-W., 2011. Synergetic effects of temperature and magnetic field on the aragonite and calcite growth. Chem. Eng. Sci. 66, 1246–1253.
Till, U., Hore, P., 1997. Radical pair kinetics in a magnetic field. Mol. Phys. 90, 289–296.
Timmel, C., Till, U., Brocklehurst, B., Mclauchlan, K., Hore, P., 1998. Effects of weak magnetic fields on free radical recombination reactions. Mol. Phys. 95, 71–89.
Tomson, M., Fu, G., Watson, M., Kan, A., 2002. Mechanisms of mineral scale inhibition. In: International Symposium on Oilfield Scale. Society of Petroleum Engineers.
Wang, P., Kosinski, J.J., Anderko, A., Springer, R.D., Lencka, M.M., Liu, J., 2013. Ethylene glycol and its mixtures with water and electrolytes: thermodynamic and transport properties. Ind. Eng. Chem. Res. 52, 15968–15987.
Yong, A., Obanijesu, E.O., 2015. Influence of natural gas production chemicals on scale production in MEG regeneration systems. Chem. Eng. Sci. 130, 172–182.
Yuan, M., Jamieson, E., Hammonds, P., 1998. Investigation of scaling and inhibition mechanisms and the influencing factors in static and dynamic inhibition tests. In: CORROSION 98. NACE International.
Zeng, B., Li, M.D., Zhu, Z.P., Zhao, J.M., Zhang, H., 2013. Application of 1-hydroxyethylidene-1, 1-diphosphonic acid in boiler water for industrial boilers. Water Sci. Technol. 67, 1544–1550.